Bioresource Technology 268 (2018) 715–725

Contents lists available at ScienceDirect

Bioresource Technology

journal homepage: www.elsevier.com/locate/biortech

Thermal degradations and processes of waste tea and tea leaves via TG-FTIR: Combustion performances, kinetics, thermodynamics, products and optimization

Haiming Cai[a], Huihuang Zou[a], Jingyong Liu[a,*], Wuming Xie[a], Jiahong Kuo[a], Musa Buyukada[b], Fatih Evrendilek[b,c]

[a] Guangzhou Key Laboratory of Environmental Catalysis and Pollution Control, School of Environmental Science and Engineering, Institute of Environmental Health and Pollution Control, Guangdong University of Technology, Guangzhou 510006, China
[b] Department of Environmental Engineering, Abant Izzet Baysal University, Bolu 14052, Turkey
[c] Department of Environmental Engineering, Ardahan University, Ardahan 75002, Turkey

GRAPHICAL ABSTRACT

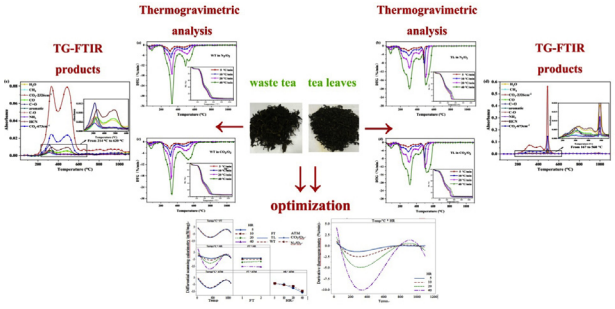

ARTICLE INFO

Keywords:
Waste tea and tea leaves
Joint optimizations
Iso-conversional methods
Combustion technology
TG–FTIR

ABSTRACT

The present study characterized the kinetic, thermodynamic and performance parameters, products, factorial interactions, and optimal conditions of combustions of waste tea (WT) and tea leaves (TL) in N_2/O_2 and CO_2/O_2 atmospheres through a thermogravimetric/Fourier transform infrared spectrometry (TG–FTIR). The main combustion occurred in the range of 200–600 °C. The increased heating rate increased all the combustion parameters regardless of the fuel and atmosphere type. Activation energy was shown different change tendency with the increasing conversion (α). CO_2, H_2O, CH_4, CO, C=O, NH_3, and HCN were the main gas products of WT and TL combustions. A three-way interaction among fuel type, atmosphere type and heating rate was found to be significant. The joint optimization of mass loss, derivative TG, and differential scanning calorimetry was achieved using 1049.3 °C, TL, 40 °C/min, and CO_2/O_2 atmosphere for the operational settings of temperature, fuel type, heating rate, and atmosphere type, respectively.

1. Introduction

Globally, biofuels and biomass wastes account for about 14% of the total energy consumption (Chen et al., 2018b). Biomass feedstock resources have been explored as the renewable and environmental friendly sources for energy generation, including cornstalk (Wen et al.,

* Corresponding author.
E-mail address: Liujy@gdut.edu.cn (J. Liu).

https://doi.org/10.1016/j.biortech.2018.08.068
Received 7 August 2018; Received in revised form 14 August 2018; Accepted 16 August 2018
Available online 18 August 2018
0960-8524/

2016), rice husk (Ma et al., 2015), para grass (Ahmad et al., 2017a), cattle manure (Yuan et al., 2017), coffee grounds (Bok et al., 2012), red pepper (Maia and Morais, 2016), water hyacinth (Huang et al., 2018b), pomelo peel (Xie et al., 2018a), and sugarcane bagasse (Xie et al., 2018b). Globally, tea is the second most widely consumed drink of the beverage industry. In 2015, China produced 42.8% of the global tea production of 5.3 million tons. The rapidly developed tea industry has now accounted for 20% of the Chinese beverage market (Zhao et al., 2018).

The deep processing by tea factories generates a large amount of unqualified tea leaves (TL), also known as refused tea, about 10% of yield (Pelvan and Özilgen, 2017). As over 90% of tea is left as waste tea (WT) after tea beverage industry (Zhong et al., 2017), the disposal and reuses of WT have been explored through composting (Ahmed et al., 2015), pyrolysis (Tian et al., 2016), and the preparation of biological carbon (Fan et al., 2016; Uzun et al., 2010) and an adsorbent to remove mercury (Shen et al., 2017).

In the face of the pressure on the environment by the vast accumulation of highly recalcitrant WT and TL, combustion as the simplest waste-treatment technology has the significant advantages of waste-stream reduction, reuse, and power generation and accounted for over 97% of the global bio-energy production (Chen et al., 2017b). The development and optimization of biomass combustion technologies necessitate the quantification of operational conditions and their relative importance. For example, the replacement of N_2 by CO_2 was reported to exert some negative effects on the performance indices of biomass combustion such as ignition, burning stability, heat transfer, gas temperature, and burnout (Chen et al., 2015). Combustion in CO_2/O_2 atmosphere was pointed out to minimize waste heat in the process, organic pollutants in exhaust gases, and the thermal energy of the exhaust gases (Huang et al., 2016). Combustion characteristics and performances of coal gangue were stated to differ in response to the oxy-fuel (CO_2/O_2) and air (N_2/O_2) atmospheres (Meng et al., 2013).

Operation conditions are analyzed using different techniques in order to characterize and optimize the combustion process and performance. For example, thermogravimetric analysis (TGA) is an effective way to better quantify the combustion, kinetic and thermodynamic parameters, and thus, to understand the thermal degradations and processes of solid biofuels (Zhuo et al., 2017). Various iso-conversional methods such as Friedman, Flynn-Wall-Ozawa (FWO) and distributed activation energy model (DAEM) were developed to estimate solid-state kinetic parameters (Chen et al., 2017a; Fang et al., 2018). TG-Fourier-transform infrared spectroscopy (FTIR) can dynamically track the composition of substances released from the complex thermal decomposition of biofuels with multiple chemical reactions (Lin et al., 2016). However, to the best of our knowledge, there exists no study about the combustion characteristics, products and performances of WT and TL in the N_2/O_2 and CO_2/O_2 atmospheres.

Therefore, the objectives of this study were to: (1) quantify the combustion performances of WT and TL in N_2/O_2 and CO_2/O_2 atmospheres by using combustion parameters; (2) estimate activation energy (E) via three iso-conversional methods; (3) determine thermodynamic changes through four indices; (4) characterize main gaseous products by using TG-FTIR; and (5) detect interaction effects of operational conditions as well as joint optimizations of the multiple responses of mass loss, derivative TG (DTG), and differential scanning calorimetry (DSC) using empirical models.

2. Materials and methods

2.1. Materials preparation

TL was sampled from those planted in the Anhui province, while WT was generated from TL samples soaked in hot water after several times. Waste tea was taken out of soaked TL and dried naturally under good ventilation for 24 h. To further remove their moisture content, the TL and WT samples were dried in an oven at 105 °C for 24 h. The samples were grounded into 200 mesh before the TG experiments. *The Proximate Analysis of Solid Biofuels of China* (GB/T 28732-2012) was adopted to carry out the proximate analysis. The ultimate analysis was performed using an elemental analyzer (Vario EL cube by Elementar). The heating values were measured with a WZR-1T-CII microcomputer calorimeter.

2.2. TGA experiment

The TGA experiments were carried out using an NETZSCH STA 409 thermal analyzer with a gas flow rate of 50 mL/min in the following two atmospheres of 79% N_2/21% O_2 and 79% CO_2/21% O_2. The four heating rates used in this study were 5, 10, 20 and 40 °C/min. The combustion temperature was increased from room temperature (RT) to about 1100 °C. The control parameters of the temperature rise, the atmosphere type, and the gas flow rate were set beforehand. The sample was put into an alumina crucible with mass of 6 ± 0.5 mg (weighed by an electronic balance) for the analyzer in each test. The real-time variation of the sample mass loss was monitored during the entire combustion process. To ensure repeatability, each experiment was conducted in triplicates.

2.2.1. TG-FTIR

The combustion products of WT and TL were analyzed using a TGA system (NETZSCH STA 409 PC Luxx, Germany) coupled with an FTIR spectrometer (TENSOR 27 FTIR, Germany). The N_2/O_2 atmosphere was used as the agent gas at a flowing rate of 50 mL/min. All the samples were kept at the weight of 6 ± 0.5 mg for reducing the heat transfer limitation. The samples were heated from RT to 1100 °C at heating rate of 20 °C/min. Moreover, the volatiles released during the combustion process were detected online using a FTIR spectrometer whose spectra were recorded from 4000 to 600 cm^{-1}. The FTIR analysis was carried out at a resolution of 4 cm^{-1}. The test data were processed using the OMNIC software (Thermo Electron, USA). To eliminate the background signal, blank experiments were carried out before the loading of the samples.

2.3. Combustion characteristics

To evaluate the combustion performances of WT and TL, the eight parameters and/or indices of ignition temperature (T_i), burnout temperature (T_b), maximum weight loss rate (-R_p), peak temperature (T_p), volatile matter release (D_v), ignition (C_i), burnout (C_b), and comprehensive combustibility (S) were used in this study. These parameters can be described as a function of the characteristic temperature and the weight loss rate as follows (Chen et al., 2015):

$$D_v = \frac{-R_p}{T_p \times T_v \times \Delta T_{1/2}} \quad (1)$$

$$C_i = \frac{-R_p}{t_i - t_p} \quad (2)$$

$$C_b = \frac{-R_p}{\Delta t_{1/2} \times t_p \times t_b} \quad (3)$$

$$S = \frac{(-R_p) \times (-R_v)}{T_i^2 \times T_b} \quad (4)$$

where $-R_p$ is maximum weight loss rate, % min^{-1}; $-R_V$ is average weight loss rate, % min^{-1}; T_V represents the initial devolatilization temperature, K; T_i is ignition temperature, K; T_p is peak temperature, K; $\Delta T_{1/2}$ is time interval at the half value of -R_p, K; T_b is burnout temperature, K. t_i, t_p, t_b, and $\Delta t_{1/2}$ represent ignition time, peak time, burnout time, and time interval at the half value of $-R_p$, respectively.

2.4. Kinetic and thermodynamic analyses

The biomass combustion is a very complex process because its chemical composition is complicate. Many reactions occur simultaneously within a fraction of second during the thermal decomposition (Maia and Morais, 2016; Chen et al., 2018a). In this study, the integral and differential methods were employed to calculate the kinetic parameters during the thermal decompositions of WT and TL. The kinetic equations can be expressed using Eq. (5):

$$\frac{d\alpha}{dt} = kf(\alpha) \tag{5}$$

where α is sample conversion rate, t is reaction time, T is actual temperature (K), k is reaction rate constant, and $f(\alpha)$ is the function of the reaction mechanism. α can be determined using Eq. (6):

$$\alpha = \frac{m_0 - m_t}{m_0 - m_f} \tag{6}$$

where m_0, m_t, and m_f is the initial, actual and end masses of the samples, respectively.

According to the Arrhenius equation, $k(T)$ was expressed as follows:

$$k(T) = Aexp\left(-\frac{E}{RT}\right) \tag{7}$$

The TG experiments were performed with the linearly increased heating rates. For the non-isothermal reactions, $\beta = dT/dt$ combining Eqs. (5) and (7) yielded the following:

$$\frac{d\alpha}{dt} = \frac{A}{\beta}exp\left(-\frac{E}{RT}\right)f(\alpha) \tag{8}$$

Based on the E estimates, it is possible to select the best kinetic model to describe the experimental data (Moussout et al., 2016). Performing the integration of Eq. (8) under the initial conditions ($\alpha = 0$, at $T = T_0$), Eq. (9) was obtained:

$$G(\alpha) = \int_0^{\alpha} \frac{d\alpha}{1-\alpha} = \int_0^{T} \frac{A}{\beta}\exp\left(-\frac{E}{RT}\right)dT \tag{9}$$

The TGA method was used to determine the kinetic parameters of A, E, and $f(\alpha)$ or $G(\alpha)$. The methods applying Eq. (8) are referred to as the differential methods while those using Eq. (9) are known as the integral methods (Yuan et al., 2017). In this study, activation energy (E) was estimated using the three iso-conversional methods of Friedman, FWO, and DAEM.

2.4.1. Friedman method

The first and more general iso-conversional method is the Friedman method. By applying the natural logarithm on both sides of Eq. (9), the following was obtained:

$$ln\beta\left(\frac{d\alpha}{dT}\right) = -\frac{E}{RT} + ln(Af(\alpha)) \tag{10}$$

In this method, the conversion function$f(\alpha)$ remains constant, thus indicating that the biomass decomposition depends only on mass loss rate being independent on temperature.

2.4.2. FWO method

In the FWO method, Eq. (9) was integrated using the Doyle's approximation for the temperature integral. The resultant equation was given below (Tran et al., 2014):

$$\ln\beta = \ln\left(\frac{AE}{RG(\alpha)}\right) - 5.3305 - 1.052\left(\frac{E}{RT}\right) \tag{11}$$

Since $\ln\left(\frac{AE}{RG(\alpha)}\right)$ does not relate to β, E was estimated as the slope of ($1.052\ E/R$) of the least square regression line plotted for $\ln\beta$ as y-axis versus 1/T as x-axis.

2.4.3. DAEM

The DAEM method is a common approach to simulate complex reactions such as co-combustion of fossil fuels and biomass (Huang et al., 2018a). Eq. (9) was rewritten thus:

$$\ln\left(\frac{\beta}{T^2}\right) = \ln\left(\frac{AR}{E}\right) + 0.6075 - \frac{E}{RT} \tag{12}$$

From Eq. (12), the plot of $\ln\left(\frac{\beta}{T^2}\right)$ versus $1/T$ gives a linear equation with E/R as its slope. $\ln\left(\frac{AR}{E}\right)$ provides an intercept value when 0.6075 is kept constant for simplicity.

The four thermodynamic parameters of A, ΔH, ΔG, and ΔS were also estimated using the following equations (Maia and Morais, 2016):

$$A = [\beta E exp(E/RT_m)]/(RT^2) \tag{13}$$

$$\Delta H = E - RT \tag{14}$$

$$\Delta G = E + RT_m ln(K_B T_m/hA) \tag{15}$$

$$\Delta S = (\Delta H - \Delta G)/T_m \tag{16}$$

where K_B is the Boltzmann constant (1.381×10^{-34} J/K); h is the Plank constant (6.626×10^{-34} J S); and T_m is peak temperature (K).

2.5. Statistical analyses

Correlation matrix was performed to detect linear relationships among the measured variables. Three-way multivariate of analysis (MANOVA) were used to detect significant interaction effects among the atmosphere type (the two levels), the heating rate (the four levels), and the fuel type (the two levels) on the three mean responses of remaining sample mass (RM, %), DTG (%/min), and DSC (mW/mg). Tukey's multiple comparison tests following general linear models (GLM) were further used to capture significant mean differences. The joint optimization of the responses as well as sensitivity analyses of the operational conditions were based on the best-fit multiple non-linear regression models. The best-fit models were chosen using a stepwise procedure at p value of 0.001 as a function of temperature (temp), fuel type (FT), atmosphere type (ATM), heating rate (HR), and their interaction and polynomial terms. Atmosphere type, FT, and HR were used in the model as the categorical variables. The goodness-of-fit and the predictive power of the models were evaluated using adjusted (R^2_{adj}) and predictive (R^2_{pred}) coefficients of determination, respectively. The joint optimal settings of the operational variables for the responses were determined maximizing the composite desirability (D) with a range of zero to one (the ideal case), the weighted geometric mean of the individual desirabilities (d). All the statistical analyses were implemented using Minitab 17.1.

3. Results and discussion

3.1. Proximate, ultimate and calorific value analyses

The proximate analysis (Table 1) showed that both moisture and volatile matter contents were higher in WT than TL, and the volatile matter content in the WT and TL was 82.31% and 74.80%, respectively. The ash and fixed carbon contents were higher in TL than WT. Their main elements were C, H and O, with the lower N and S contents. The calorific values of WT and TL (20.86 and 19.69 MJ/kg, respectively) were higher than those of common crop parts such as corn stalk (17.56 MJ/kg), and wheat-straw (17.45 MJ/kg) (Wen et al., 2016). These results point to the promising potential of the WT and TL combustions for energy generation.

3.2. Thermogravimetric analysis

Fig. 1(a–d) shows the (D)TG curves of WT and TL at the heating

Table 1
Proximate, ultimate and calorific value analyses of WT and TL.

Samples	Ultimate analysis (wt. %)					Proximate analysis (wt. %)				Q_{net} (MJ/kg)
	C_{ad}	H_{ad}	O_{ad}	N_{ad}	S_{ad}	M_{ad}	V_{ad}	A_{ad}	FC_{ad}	
WT	47.99	6.60	28.73	4.90	0.18	5.45	82.31	6.15	6.09	20.86
TL	47.32	5.88	30.33	4.16	0.12	4.37	74.80	7.82	12.91	19.69

ad, air-dry basis; O_{ad}, calculated by O_{ad} (%) = 100%-C_{ad}-H_{ad}-N_{ad}-S_{ad}- M_{ad}- A_{ad} (Chen et al., 2016); M_{ad}, moisture content; V_{ad}, volatile matter content; A_{ad}, ash content; FC_{ad}, fixed carbon content; and Q_{net}, calorific value.

rates of 5, 10, 20, and 40 °C/min in both atmospheres. The increased heating rate caused the TG curves and DTG peak to move to a higher temperature region, not changing the patterns of the thermal decompositions of TL and WT. This appeared to be related to the thermal hysteresis effect since the higher heating rate induced lowered heat transfer efficiency, as was generally reported in the TGA results (Zhou et al., 2017).

The combustion characteristics of WT and TL in the N_2/O_2 and CO_2/O_2 atmospheres at a heating rate of 20 °C/min are presented Fig. 1(e, f) and Table 2. The combustions in the two atmospheres were divided into three stages. As for the WT combustion, the first stage was the water loss. Its main weight losses by 54.69% and 49.52% occurred at the second stage in the ranges of 207.3–397.5 °C and 202.5–401.2 °C, respectively. These weight losses were attributed to the thermal degradation of volatiles such as hemi-celluloses, celluloses and partial lignin (Chen et al., 2017a). The maximum weight loss rates were estimated at 17.02%/min at 328.6 °C and 16.76%/min at 326.3 °C in the N_2/O_2 and CO_2/O_2 atmospheres, respectively, in the second stage. In stage III, the weight loss was associated with the decomposition of fixed carbon, lignin and other organic matters. Similarly, this stage was reported to involve the combustion of fixed carbon and residual volatiles with stronger chemical bonds such as aromatic compounds (Huang et al., 2018a). At above 637 °C, the weight loss was caused by the slow thermal decomposition of minerals.

The combustion process of TL exhibited a lower amount of weight loss than did that of WT although its weight loss in the second stage was similarly attributed to the decomposition of its hemicellulose and lignin. This was related to the higher cellulose content of WT than TL. The cellulose and crude protein contents of WT were found to increase when WT was obtained from soaked TL (Wang et al., 2016). The third stage of TL had an additional larger peak on the DTG curve of weight loss. This peak may be caused by the rapid decompositions of large amounts of fixed carbon and the volatiles produced by the second decomposition of tar, as was also reported for the decomposition of tea polyphenols (Yao et al., 2017).

The replacement of N_2 by CO_2 had similar effects on the WT and TL combustions. As shown in Fig. 1(e, f), the atmosphere type had no significant effect on the (D)TG curves at below 450 °C. At above 500 °C, the peak weight loss rate was higher in the N_2/O_2 than CO_2/O_2 atmosphere, and the replacement of N_2 by CO_2 postponed the locations of the peaks. CO_2 has higher density and heat capacity than N_2, thus absorbing more heat from the combustion furnace. Therefore, in the process of heating, more heat was removed by the carrier gas of CO_2 which resulted in lower surface temperatures of WT and TL (Wall et al., 2009). As shown in Table 2, the samples underwent a more thorough combustion in the N_2/O_2 than CO_2/O_2 atmosphere given the lower residues of WT and TL in the N_2/O_2 atmosphere. This case agreed well with mass loss rates obtained by (Tang et al., 2013). Replacing N_2 by CO_2 at the same concentration was reported to lower flame propagation speed, flame stability, and gas temperature, thus increasing the unburned carbon content in the CO_2 atmosphere (Chen et al., 2015). Our finding of the lower residues supported the reduction aimed for the WT and TL volumes.

3.3. Combustion characteristics

To better understand effects of the heating rate on the combustion performances of WT and TL in both atmospheres, the eight combustion characteristic parameters are presented in Table 3. With the increased heating rate, all the eight combustion parameters increased in both atmospheres regardless of the fuel type. Pearson's correlation matrix was performed for each atmosphere and each fuel type ($n = 4$). For both atmospheres as well as both fuel types, the heating rate had a significantly positive correlation with $-R_p$ ($p \leq 0.004$), C_i ($p \leq 0.04$), and S ($p \leq 0.02$), but no significantly positive correlation with T_i, T_p, and C_b ($p > 0.05$). The increases in T_b in both atmospheres as a function of the increased heating rate were significant only for TL ($p \leq 0.01$). Only the D_v value of WT in the CO_2/O_2 atmosphere was not significantly correlated with the heating rate. The increased heating rate postponed the decomposition process. The better comprehensive combustion performances with the increased heating rate were supported by Zhou et al. (2017). As for the impact of the atmosphere type on the WT and TL combustion characteristics (Table 3), Tukey's multiple comparison tests showed significant mean differences only in T_i and T_b ($n = 16$; $p < 0.001$). In both atmospheres, the mean T_i values of WT were significantly higher than those of TL. The mean T_b value of WT in the CO_2 atmosphere was higher than those of TL in both atmospheres.

3.4. Kinetic estimates

The model-free methods without the assumption of mechanism functions involved have gained popularity in estimating more reliable E (Tian et al., 2016). The E values of the WT and TL combustions were estimated using the three iso-conversional methods of Friedman, FWO, and DAEM in both atmospheres as a function of the conversion rate (α). The apparent E values, and their associated R^2 values are shown in Table 4 and Fig. 2. The E values were negatively correlated with α values ($r = -0.51$; $n = 108$; $p < 0.001$). The mean highest E value (240.6 ± 29 kJ/mol) at α = 0.4 (which was similar at α = 0.2, 0.3, and 0.5) was significantly different from the mean lowest E value (120.6 ± 22 kJ/mol) at α = 0.7 (which was similar at α = 0.6) ($n = 108$; $p < 0.001$). A significant variation in E with the conversion rate was found to point to a kinetically complex process (López-González et al., 2017). The impacts of the atmosphere types on the WT and TL combustions were also reflected in their E values. The change from N_2/O_2 to CO_2/O_2 atmosphere was found to significantly decrease the E values from 204.9 ± 49 to 176.2 ± 45 kJ/mol ($r = -0.29$; $n = 108$; $p = 0.002$). A similar finding was also reported about the combustion of swine manure (López-González et al., 2017). The lower E values also indicate an easily converted biofuel that can be also used in co-firing with other biofuel types with either lower or higher E values.

In terms of the kinetic models and the fuel types, the mean E values did not differ significantly ($n = 108$; $p > 0.05$). The mean R^2 values were estimated at 95.5, 97.8 and 97.6 for the Friedman, FWO, and DAEM methods, respectively, thus confirming the admissible accuracy of the results. According to Tukey's multiple comparison test, the mean R^2 values of the FWO and DAEM methods were higher than that of the Friedman method ($n = 108$; $p = 0.017$). For the FWO method, the

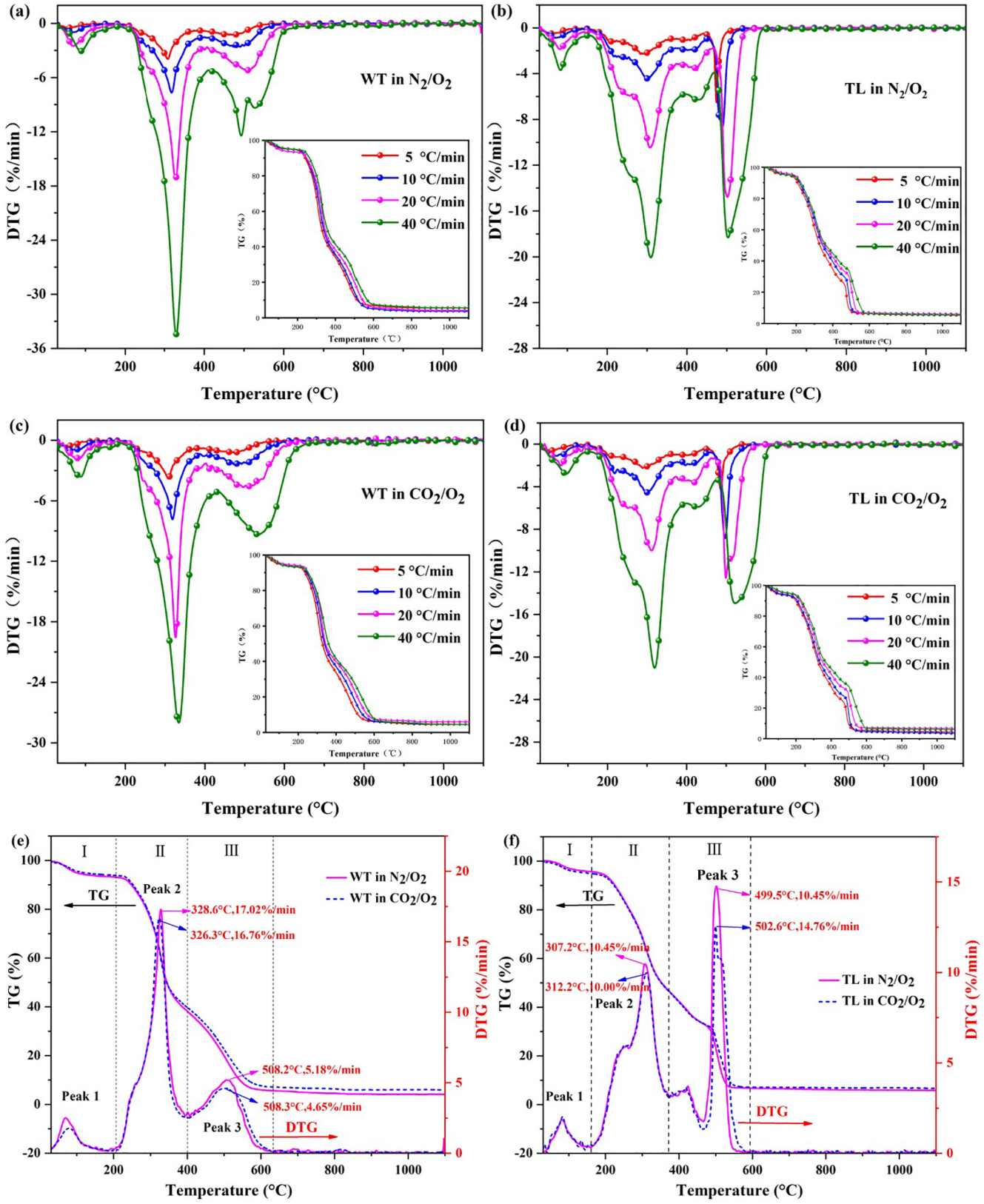

Fig. 1. (D)TG curves at four heating rates: (a) WT and (b) TL combustions in N_2/O_2 atmosphere; (c) WT and (d) TL combustions in CO_2/O_2 atmosphere; and (D)TG curves of (e) WT and (f) TL combustions at 20 °C/min as a function of temperature.

dependence of the apparent E on α can be separated into the two distinct regions. The first region had the stable E values in the α range of 0.1 to 0.5. The second region had a slight E variation for WT, but a substantial increase for TL in the α range of 0.6 to 0.9. The two regions corresponded to our earlier discussions about the DTG plots. The first stage belonged to the release of volatiles during which hemi-celluloses, celluloses and some portion of lignin were decomposed. The second stage was the decomposition of other oxides or inorganic substances.

Table 2
Three decomposition stages of WT and TL, and their associated temperature ranges, weight losses and residues at 20 °C/min.

Atmosphere	Sample	I		II		III		Residue (%)
		Temperature range (°C)	Weight loss (%)	Temperature range (°C)	Weight loss (%)	Temperature range (°C)	Weight loss (%)	
N_2/O_2	WT	41.0–207.3	6.56	207.3–397.5	54.69	397.5–633.7	33.11	4.21
	TL	40.3–167.2	4.44	167.2–372.0	48.86	372.0–577.5	39.74	5.98
CO_2/O_2	WT	42.5–202.5	6.06	202.5–401.2	54.28	401.2–637.6	32.55	5.97
	TL	42.2–169.8	4.64	169.8–377.2	49.52	377.2–593.3	38.65	6.89

Table 3
Combustion characteristic parameters of WT and TL as a function of heating rate in N_2/O_2 and CO_2/O_2 atmospheres.

Atmosphere	Sample	β	T_i	$-R_p$	T_p	T_b	C_i	D_v	C_b	S
N_2/O_2	WT	5	277.8	3.94	308.7	550.1	0.14	1.14	0.06	0.41
		10	280.1	7.66	318.2	573.2	1.02	1.90	0.84	1.57
		20	289.8	17.29	328.0	595.0	8.31	4.95	18.87	6.61
		40	294.2	34.44	329.6	605.4	57.45	8.45	263.84	26.06
	TL	5	236.1	2.28	283.8	511.2	0.10	0.39	0.02	0.36
		10	249.3	4.45	302.2	514.6	0.71	0.63	0.25	1.26
		20	255.2	10.46	307.4	533.2	6.05	1.89	5.72	5.73
		40	257.1	20.06	309.6	566.2	39.47	3.11	76.29	21.25
CO_2/O_2	WT	5	266.2	3.80	308.3	571.0	0.14	1.08	0.06	0.42
		10	279.9	7.94	318.8	599.5	1.06	2.32	0.92	1.54
		20	285.5	16.26	329.5	610.1	7.88	4.52	16.40	6.28
		40	287	28.00	334.4	632.6	47.42	5.34	159.52	21.09
	TL	5	231.1	2.24	289.5	521.1	0.10	0.33	0.02	0.36
		10	241.9	4.54	300.2	539.1	0.75	0.64	0.26	1.33
		20	251.8	10.00	311.7	544.3	5.80	1.52	4.39	5.37
		40	253.0	21.02	319.3	585.7	40.93	3.23	81.70	21.81

β is heating rate, °C/min; T_i is ignition temperature, °C; $-R_p$ is maximum weight loss rate, %/min; T_b is burnout temperature, °C; T_p is peak temperature, °C; C_b is burnout index, $10^{-3}\cdot(\%\cdot min^{-4})$; S is comprehensive combustibility index, $10^{-7}\cdot(\%^{2}\cdot°C^{-3}\cdot min^{-2})$; D_v is volatile matter release index, $10^{-6}\cdot(\%\cdot min^{-1}\cdot°C^{-3})$; and C_i is ignition index, $10^{-2}\cdot(\%\cdot min^{-3})$.

Our result was consistent with the finding about Turkish lignite (Selcuk and Yuzbasi, 2011).

3.5. Thermodynamic parameters

To estimate the thermodynamic parameters of the combustion processes plays an important role in the large-scale design of combustion reactors as well as in the selection of suitable biofuels. The A, ΔH, ΔG and ΔS estimates by the FWO method in both atmospheres at 20 °C/min are shown in Table 5 and Fig. 3. The mean A values did not significantly differ in terms of the atmosphere and fuel types, and the conversion rate ($n = 36$; $p > 0.05$). The A estimates of TL and WT were

Table 4
Activation energies (E, kJ/mol) of WT and TL combustions as a function of conversion rate according to Friedman, FWO, and DAEM in N_2/O_2 and CO_2/O_2 atmosphere.

Atmosphere	α	WT						TL					
		Friedman		FWO		DAEM		Friedman		FWO		DAEM	
		E	R^2	E	R^2	E	R^2	E	R^2	E	R^2	E	R^2
N_2/O_2	0.10	219.46	0.950	195.57	0.914	196.95	0.906	206.47	0.972	193.32	0.952	195.18	0.948
	0.20	242.34	0.998	218.48	0.990	220.46	0.989	294.06	0.933	253.92	0.946	258.26	0.942
	0.30	253.03	0.976	223.26	0.997	225.14	0.996	281.32	0.922	256.88	0.936	260.84	0.932
	0.40	255.28	0.971	231.81	0.978	233.91	0.976	302.70	0.949	268.44	0.946	272.65	0.942
	0.50	245.45	0.966	227.43	0.989	229.04	0.988	192.02	0.979	228.60	0.986	230.30	0.984
	0.60	149.78	0.991	177.30	0.992	175.81	0.991	126.79	0.999	134.90	0.997	130.93	0.997
	0.70	153.44	0.995	145.46	1.000	141.31	1.000	111.80	0.845	102.65	0.998	96.01	0.997
	0.80	202.09	0.965	178.28	0.987	175.08	0.985	246.78	0.862	203.71	0.997	201.56	0.996
	0.90	200.37	0.999	187.25	0.997	183.85	0.996	124.24	0.926	203.92	0.990	201.58	0.988
	Average	213.47	0.979	198.32	0.983	197.95	0.981	209.58	0.932	205.15	0.972	205.26	0.970
CO_2/O_2	0.10	260.76	0.924	243.66	0.907	247.62	0.901	146.78	0.995	131.92	0.996	130.62	0.995
	0.20	246.32	0.966	232.40	0.969	235.15	0.966	201.38	0.997	166.03	0.997	165.81	0.997
	0.30	238.34	0.983	223.39	0.983	225.30	0.982	210.57	0.999	188.61	0.999	189.04	0.999
	0.40	223.01	0.958	214.05	0.993	215.20	0.992	245.78	0.999	211.94	0.999	213.19	0.999
	0.50	204.61	0.893	201.43	0.952	201.64	0.947	163.86	0.970	193.37	0.985	194.04	0.984
	0.60	135.92	0.994	159.92	0.966	157.43	0.961	110.06	0.981	121.37	0.987	116.67	0.985
	0.70	138.43	0.996	135.16	0.994	130.39	0.993	98.21	0.946	100.92	0.986	94.17	0.982
	0.80	152.35	0.996	145.50	0.995	140.44	0.993	213.27	0.793	175.96	0.981	172.17	0.978
	0.90	163.72	0.991	155.14	0.993	149.87	0.992	88.8	0.824	149.71	0.956	144.19	0.947
	Average	195.94	0.967	190.07	0.972	189.23	0.970	164.30	0.945	159.98	0.987	157.77	0.985

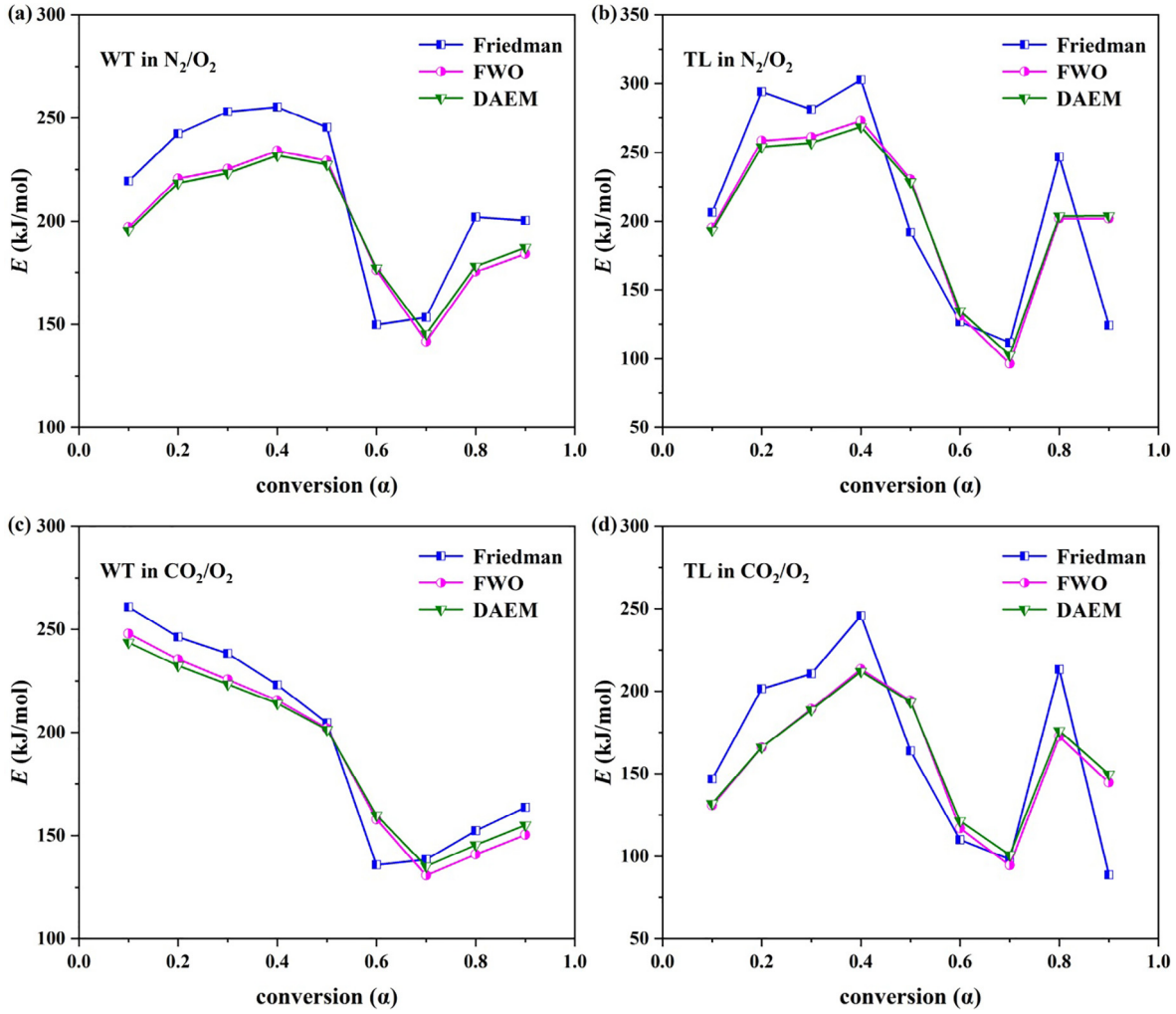

Fig. 2. Changes in activation energy (E) of (a) WT and (b) TL combustions in N_2/O_2 atmosphere; (c) WT and (d) TL combustions in CO_2/O_2 atmosphere as a function of conversion rate based on Friedman, FWO and DAEM methods.

Table 5
Thermodynamic parameters of WT and TL combustions as a function of conversion rate at 20 °C/min in N_2/O_2 and CO_2/O_2 atmospheres according to FWO.

Atmosphere	α	WT				TL			
		A (S^{-1})	ΔH (kJ/mol)	ΔG (kJ/mol)	ΔS (J/mol)	A (S^{-1})	ΔH (kJ/mol)	ΔG (kJ/mol)	ΔS (J/mol)
N_2/O_2	0.1	1.30×10^{17}	191.24	128.92	103.70	3.46×10^{17}	189.20	124.05	112.25
	0.2	1.42×10^{19}	213.82	128.36	142.20	1.29×10^{23}	249.48	122.73	218.38
	0.3	3.77×10^{19}	218.40	128.26	149.99	2.41×10^{23}	252.18	122.68	223.12
	0.4	2.17×10^{20}	226.82	128.07	164.31	2.77×10^{24}	263.56	122.47	243.10
	0.5	8.85×10^{19}	222.32	128.16	156.67	6.13×10^{20}	223.56	123.24	172.84
	0.6	3.04×10^{15}	171.94	129.41	70.76	1.33×10^{12}	129.37	125.79	6.17
	0.7	4.26×10^{12}	139.55	130.40	15.23	1.27×10^{9}	96.59	127.10	−52.57
	0.8	3.71×10^{15}	171.97	129.38	70.86	3.14×10^{18}	197.30	123.80	126.63
	0.9	2.35×10^{16}	180.41	129.14	85.32	3.28×10^{18}	197.39	123.79	126.81
	Average	–	192.94	128.90	106.56	–	199.85	123.96	130.75
CO_2/O_2	0.1	2.16×10^{21}	239.30	128.18	184.44	5.66×10^{11}	127.82	126.93	1.51
	0.2	2.17×10^{20}	227.72	128.41	164.83	7.94×10^{14}	161.60	125.82	61.20
	0.3	3.45×10^{19}	218.53	128.61	149.24	9.41×10^{16}	183.92	125.20	100.44
	0.4	5.12×10^{18}	209.07	128.83	133.19	1.28×10^{19}	207.06	124.63	140.98
	0.5	3.88×10^{17}	196.35	129.13	111.57	2.56×10^{17}	188.29	125.08	108.11
	0.6	7.76×10^{13}	154.55	130.29	40.27	5.94×10^{10}	115.86	127.34	−19.63
	0.7	4.68×10^{11}	129.22	131.13	−3.17	7.37×10^{8}	94.91	128.24	−56.99
	0.8	3.97×10^{12}	139.15	130.76	13.93	6.49×10^{15}	169.51	125.53	75.20
	0.9	2.90×10^{13}	148.44	130.44	29.88	2.50×10^{13}	143.11	126.32	28.72
	Average	–	184.70	129.53	91.58	–	154.68	126.12	48.84

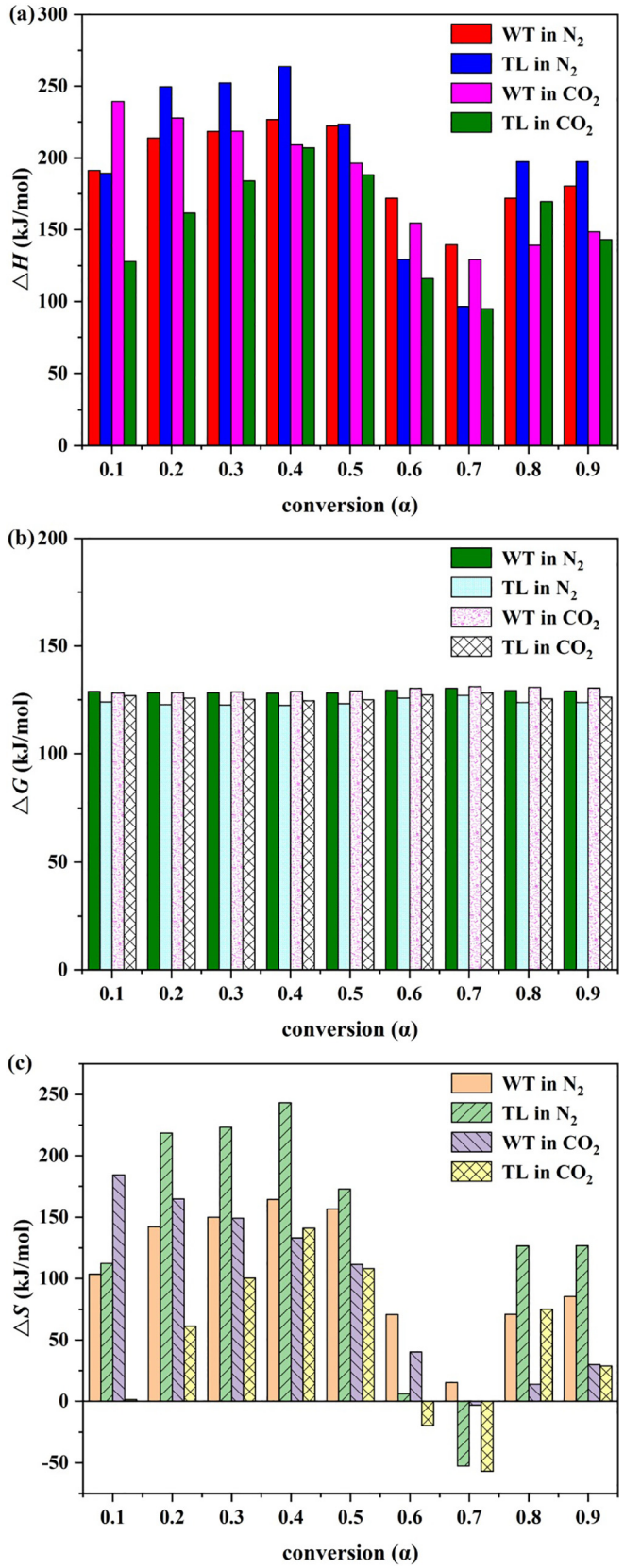

Fig. 3. Thermodynamic parameters of WT and TL combustions at 20 °C/min in N_2/O_2 and CO_2/O_2 atmospheres as a function of conversion rate according to FWO: (a) ΔH, (b) ΔG and (c) ΔS.

close to those of para grass (2.55×10^8 to $2.26 \times 10^{19}\ s^{-1}$), and cattle manure ($5.47 \times 10^9$ to $1.33 \times 10^{30}\ s^{-1}$) (Ahmad et al., 2017a; Yuan et al., 2017). The lower A values ($< 10^9\ s^{-1}$) indicate a surface reaction. If the reactions are independent on the surface area, the lower A values may also indicate a closed complex. However, the higher A values ($> 10^9\ s^{-1}$) show a simple complex (Turmanova1 et al., 2008). The wide range of the A values of WT and TL pointed to their complex structure with multiple stages of chemical reactions during their combustion.

The ΔH values illustrate the energy difference between the reagent and the activated complex (Huang et al., 2018b). The ΔH values were negatively correlated with the α values ($r = -0.49$; $n = 36$; $p = 0.002$). The mean highest H value at α = 0.4 (226.6 ± 26 kJ/mol) (similar at α = 0.1 to 0.5, 0.8 and 0.9) was significantly different from the mean lowest ΔH value at α = 0.7 (115.1 ± 22 kJ/mol) (similar at α = 0.6) ($n = 36$; $p < 0.001$). A low potential energy barrier (5–7 kJ/mol) was found when ΔH was compared with the E values of WT and TL which reflected the feasibility of reactions (Gan et al., 2018). The low difference between the E and ΔH values was stated to easily achieve the product formation (Ahmad et al., 2017b).

The ΔG values indicated the total energy increase of the reaction mechanism in terms of the reagents, and the formation of the activated complex. A higher ΔG value represents a lower reaction favorability (Huang et al., 2016). Unlike the other thermodynamic parameters, only the change from WT to TL was found to significantly decrease the ΔG value from 129.2 ± 0.9 to 125.0 ± 1.7 kJ/mol ($r = -0.83$; $n = 36$; $p < 0.001$). The ΔS value as a measure of disorder indicates the disorder degree of products produced via bond dissociation when positive and is higher for the products than the initial reactants (He et al., 2018). As shown in Fig. 3c, the dominancy of the positive ΔS values of the WT and TL combustions pointed to their enhanced disorder degrees. Similar results were pointed out for para grass (−122.23 to 94.38 J/mol) (Ahmad et al., 2017a), red pepper (−249.52 to −8.31 J/mol) (Maia and Morais, 2016), and cattle manure (−71.23 to 316.19 J/mol) (Yuan et al., 2017). The ΔS values were also negatively correlated with the α values ($r = -0.48$; $n = 36$; $p = 0.002$). As with ΔH, the mean highest ΔS value at α = 0.4 (170.4 ± 50 J/mol) (similar at α = 0.1 to 0.5, 0.8 and 0.9) was significantly different from the mean lowest ΔS value at α = 0.7 (−24.4 ± 35 J/mol) (similar at α = 0.6) ($n = 36$; $p < 0.001$). Thermodynamic parameters play an important role in combustion reactor design for the large-scale combustion process and in selection of suitable biomass species.

3.6. TG-FTIR results

FTIR is often used to distinguish the various (in)organic compounds after the thermal degradation. The produced gases can be confirmed by matching characteristic peaks of a spectrogram to functional groups (Zhang et al., 2018). The peak intensity of a specific wavenumber represented the release intensity of the combustion products (Granada et al., 2012). The variation of the spectral intensity was similar to that of the DTG curves over time. As other biofuels did, WT and TL contained natural macromolecular polymers such as hemi-celluloses, celluloses and lignin. With the focus on the maximum weight loss rate of the main stage, the gas products of WT and TL were identified in the combustions process. The main volatile components identified were small molecular gases and included H_2O, CH_4, CO_2, CO, aromatic, C—O, NH_3, HCN, and light tar components (C═O) such as aldehydes, ketones, and acids. The absorbance peaks at 3456, 2927, 2326 (673), 2179, 1374, 1170, 966 and 714 cm^{-1} corresponded to the releases of H_2O, CH_4, CO_2, CO, aromatic, C—O, NH_3, and HCN, respectively. The absorbance peak at 1786 cm^{-1} was attributed to the releases of aldehydes, ketones, and acids (C═O) (Ma et al., 2015; Tang et al., 2017; Xie et al., 2018a).

The main combustion products of WT and TL appeared in the ranges of 200 to 600 °C and 205 to 560 °C, respectively. The releases of CH_4,

C═O, aromatics, C−O, and NH_3 mainly occurred in the range of 200 to 400 °C, with maximum release temperatures at 328.6 °C for WT and 307.2 °C for TL. Other products such as H_2O, CO_2, CO and HCN were released during the main combustion process. The release intensity of H_2O form WT was higher than TL at the main reaction stage. H_2O released mainly from the evolution of bulk water, bound water, and crystallization water in the mineral substance. With the increased temperature, H_2O also stemmed from the cracking or reaction of oxygen functional groups (Liang et al., 2018). The evolutions of CH_4, CO_2, and CO were mainly attributed to the cleavage of functional groups such as methoxyl group, and ether group (R-O-R, carboxyl and carbonyl group (C═O)) as well as to the secondary cracking of phenolic compounds (Zhao et al., 2014). The release intensity of CH_4 was relatively low in the entire combustions. The release intensity of CO was similar to that of H_2O, but was lower in the TL than WT combustion.

The releases of C═O, aromatic, and C−O such as carbonyls, acids, phenol, ether, and alcohol occurred mainly in the range of 200 to 400 °C. At the lower temperatures, C═O was usually produced by the fracture of the O-acetyl side chain of the hemi-cellulose structure (Tian et al., 2016). The fragmentation of methoxy was the main source of the methanol formation in the lignin combustion process, with $-CH_2OH$ group on the alkyl side chain as another source of alcohol (Wang et al., 2009). Their intensity was higher for WT than TL which was attributed to the increased organic matter content of WT after the process of soaking. The intensities of aromatic were similar to those of C-O for WT and TL. NH_3 were also detected although its intensity was not obvious. The HCN releases from WT and TL were mainly in the ranges of 200 to 595 °C and 205 to 560 °C, respectively. Its higher intensity from TL in the range of 470–560 °C may be caused by the rapid decomposition of large amounts of fixed carbon, and the volatiles of the second decomposition.

3.7. Interaction effects of operational parameters

An interaction effect exists when response(s) at a factor level depend(s) on the levels of the other factors. The three alternative tests of the three-way MANOVA pointed consistently to a three-way interaction effect of atmosphere type, fuel type, and heating rate on the responses of mass loss, DTG, and DSC (Wilk's lambda = 0.908, $F = 1863$; Lawley-Hotelling trace = 0.100, $F = 1917$; Pillai's trace = 0.091, $F = 1796$; df = 9; $n = 171010$; $p < 0.001$). All the significantly different pairwise comparisons were further displayed in Table 6. The interaction plots in

Table 6
Tukey's multiple comparisons of mean responses of remaining mass (RM, %), DSC (mW/mg), and DTG (%/min) as a function of three-way interactions between atmosphere type (ATM), fuel type (FT), and heating rate (HR) ($n = 171010$).

ATM	FT	HR	n	Mean RM	Mean DSC	Mean DTG
CO_2/O_2	TL	5	10,692	31.6 g	−1.50 cd	−0.45 a
CO_2/O_2	TL	10	10,695	32.3 fg	−2.54 e	−0.92 b
CO_2/O_2	TL	20	10,689	35.6 abc	−6.13 i	−1.85 c
CO_2/O_2	TL	40	10,687	36.9 a	−5.03 h	−3.89 d
CO_2/O_2	WT	5	10,692	32.5 efg	−1.31 bcd	−0.45 a
CO_2/O_2	WT	10	10,695	34.0 cdef	−0.72 a	−0.91 b
CO_2/O_2	WT	20	10,694	35.7 ab	−4.77 h	−1.85 c
CO_2/O_2	WT	40	10,686	36.0 a	−11.05 k	−3.94 d
N_2/O_2	TL	5	10,688	32.4 efg	−1.19 bc	−0.45 a
N_2/O_2	TL	10	10,688	34.1 bcde	−1.57 d	−0.90 b
N_2/O_2	TL	20	10,678	35.2 abc	−2.61 ef	−1.90 c
N_2/O_2	TL	40	10,688	35.7 abc	−8.99 j	−3.96 d
N_2/O_2	WT	5	10,688	33.3 defg	−1.10 b	−0.44 a
N_2/O_2	WT	10	10,688	33.1 defg	−3.68 g	−0.92 b
N_2/O_2	WT	20	10,673	34.3 bcd	−2.87 f	−1.91 c
N_2/O_2	WT	40	10,689	36.4 a	−4.81 h	−3.96 d

Means in the columns that do not share the same letter are significantly different at $p < 0.001$.

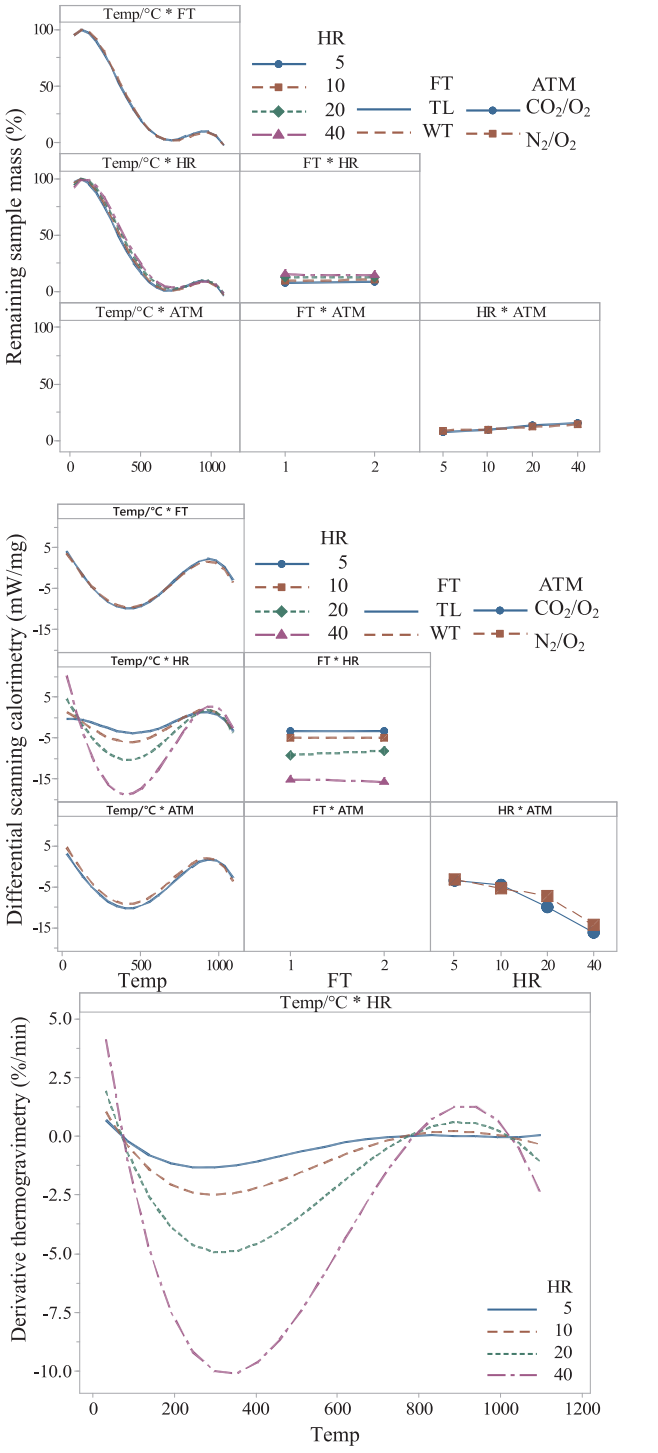

Fig. 4. Plots of two-way interaction effects of fuel type (FT), atmosphere type (ATM), heating rate (HR, K/min), and temperature (Temp, °C) on the responses based on the best-fit models ($p = 0.001$).

Fig. 4 based on the best-fit models also show significant two-way interactions ($p = 0.001$). Out of all the combinations, only the temperature by atmosphere type and fuel type by atmosphere type interactions were not significant for mass loss, while only the latter was not significant for DSC (Fig. 4). On DTG, only the interaction effect of temperature and heating rate was found to be significant (Fig. 4).

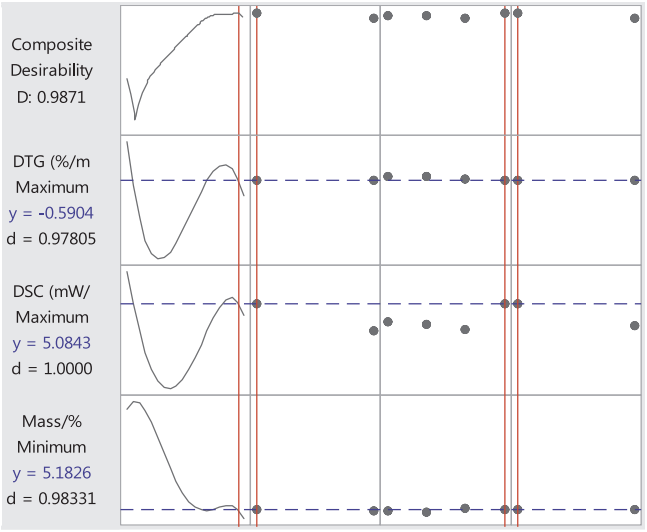

Fig. 5. The vertical red and horizontal blue lines represent the optimal factor settings (levels), and their response (y) values, respectively. (For interpretation of the references to colour in this figure legend, the reader is referred to the web version of this article.)

3.8. Joint optimization and sensitivity analysis of multiple responses

The best-fit multiple non-linear regression models (please see supplementary information) accounted for 98.8, 64.3 and 56.9% of variations in the remaining sample mass (%) (SE = 3.9), DSC (mW/mg) (SE = 4.2), and DTG (%/min) (SE = 2.3), respectively (n = 171010; p = 0.001). Based on the joint optimization of the best-fit models of the three responses, the optimal operational settings were estimated at 1049.3 °C for temperature, TL for the fuel type, CO_2/O_2 for the atmosphere type, and 40 °C/min for the heating rate (D = 0.987) (Fig. 5). The optimal settings for the second best optimization were determined as 823.3 °C, WT, CO_2/O_2, and 10 °C/min (D = 0.982). The optimal factor settings were predicted under the assumption that each operational factor carried the same weight of importance.

Given the joint optimization achieved under the above conditions, the sensitivity analysis of the three categorical variables was carried out using the *ceteris paribus* approach. The composite desirability of the joint optimization was found to be most and least sensitive to the changes in the heating rate and the atmosphere type, respectively. The lowest D values showed a slight variation with 0.943, 0945 and 0.949 in response to the changing factor levels of heating rate, fuel type, and atmosphere type, respectively, relative to that of the joint optimization (0.987).

4. Conclusions

The main combustions occurred at 200–600 °C. The average activation energies of both WT and TL combustions were higher in the N_2/O_2 than CO_2/O_2 atmosphere. H_2O, CH_4, CO, CO_2, NH_3 and HCN were identified as the main gaseous evolutions from the combustions. Significant three-way and two-way interactions among the fuel and atmosphere types, the heating rate, and temperature were found simultaneously on the three responses. The best and second best joint optimizations were achieved in the CO_2/O_2 atmosphere with the following factor settings of 1049.3 and 823.3 °C, TL and WT, 40 and 10 °C/min, respectively.

Acknowledgments

This research was financially supported by the Scientific and Technological Planning Project of Guangzhou, China (Nos. 201704030109 & 2016201604030058), and the Science and Technology Planning Project of Guangdong Province, China (Nos. 2017A050501036, 2017A040403063 & 2017A040403059), and Guangdong Special Support Program for Training High Level Talents (No.2014TQ01Z248).

References

Ahmad, M.S., Mehmood, M.A., Al Ayed, O.S., Ye, G., Luo, H., Ibrahim, M., Rashid, U., Arbi Nehdi, I., Qadir, G., 2017a. Kinetic analyses and pyrolytic behavior of Para grass (Urochloa mutica) for its bioenergy potential. Bioresour. Technol. 224, 708–713.

Ahmad, M.S., Mehmood, M.A., Taqvi, S.T.H., Elkamel, A., Liu, C.-G., Xu, J., Rahimuddin, S.A., Gull, M., 2017b. Pyrolysis, kinetics analysis, thermodynamics parameters and reaction mechanism of Typha latifolia to evaluate its bioenergy potential. Bioresour. Technol. 245, 491–501.

Ahmed, S.T., Lee, J.W., Mun, H.S., Yang, C.J., 2015. Effects of supplementation with green tea by-products on growth performance, meat quality, blood metabolites and immune cell proliferation in goats. J. Anim. Physiol. Anim. Nutr. 99 (6), 1127–1137.

Bok, J.P., Choi, H.S., Choi, Y.S., Park, H.C., Kim, S.J., 2012. Fast pyrolysis of coffee grounds: characteristics of product yields and biocrude oil quality. Energy 47, 17–24.

Chen, J., Liu, J., He, Y., Huang, L., Sun, S., Sun, J., Chang, K., Kuo, J., Huang, S., Ning, X., 2017a. Investigation of co-combustion characteristics of sewage sludge and coffee grounds mixtures using thermogravimetric analysis coupled to artificial neural networks modeling. Bioresour. Technol. 225, 234–245.

Chen, X., Liu, L., Zhang, L., Zhao, Y., Zhang, Z., Xie, X., Qiu, P., Chen, G., Pei, J., 2018b. Thermogravimetric analysis and kinetics of the co-pyrolysis of coal blends with corn stalks. Thermochim. Acta 659, 59–65.

Chen, J., Mu, L., Cai, J., Yao, P., Song, X., Yin, H., Li, A., 2015. Pyrolysis and oxy-fuel combustion characteristics and kinetics of petrochemical wastewater sludge using thermogravimetric analysis. Bioresour. Technol. 198, 115–123.

Chen, N., Ren, J., Ye, Z., Xu, Q., Liu, J., Sun, S., 2016. Kinetics of coffee industrial residue pyrolysis using distributed activation energy model and components separation of bio-oil by sequencing temperature-raising pyrolysis. Bioresour. Technol. 221, 534–540.

Chen, J., Wang, Y., Lang, X., Ren, X., Fan, S., 2017b. Comparative evaluation of thermal oxidative decomposition for oil-plant residues via thermogravimetric analysis: thermal conversion characteristics, kinetics, and thermodynamics. Bioresour. Technol. 243, 37–46.

Chen, J., Xie, C., Liu, J., He, Y., Xie, W., Zhang, X., Chang, K., Kuo, J., Sun, J., Zheng, L., Sun, S., Buyukada, M., Evrendilek, F., 2018a. Co-combustion of sewage sludge and coffee grounds under increased O_2/CO_2 atmospheres: thermodynamic characteristics, kinetics and artificial neural network modeling. Bioresour. Technol. 250, 230–238.

Fan, S., Tang, J., Wang, Y., Li, H., Zhang, H., Tang, J., Wang, Z., Li, X., 2016. Biochar prepared from co-pyrolysis of municipal sewage sludge and tea waste for the adsorption of methylene blue from aqueous solutions: kinetics, isotherm, thermodynamic and mechanism. J. Mol. Liq. 220, 432–441.

Fang, S., Yu, Z., Ma, X., Lin, Y., Chen, L., Liao, Y., 2018. Analysis of catalytic pyrolysis of municipal solid waste and paper sludge using TG-FTIR, Py-GC/MS and DAEM (distributed activation energy model). Energy 143, 517–532.

Gan, D.K.W., Loy, A.C.M., Chin, B.L.F., Yusup, S., Unrean, P., Rianawati, E., Acda, M.N., 2018. Kinetics and thermodynamic analysis in one-pot pyrolysis of rice hull using renewable calcium oxide based catalysts. Bioresour. Technol. 265, 180–190.

Granada, E., Eguía, P., Vilan, J.A., Comesaña, J.A., Comesaña, R., 2012. FTIR quantitative analysis technique for gases. Application in a biomass thermochemical process. Renewable Energy 41, 416–421.

He, Y., Chang, C., Li, P., Han, X., Li, H., Fang, S., Chen, J., Ma, X., 2018. Thermal decomposition and kinetics of coal and fermented cornstalk using thermogravimetric analysis. Bioresour. Technol. 259, 294–303.

Huang, L., Liu, J., He, Y., Sun, S., Chen, J., Sun, J., Chang, K., Kuo, J., Ning, X., 2016. Thermodynamics and kinetics parameters of co-combustion between sewage sludge and water hyacinth in CO_2/O_2 atmosphere as biomass to solid biofuel. Bioresour. Technol. 218, 631–642.

Huang, J., Liu, J., Chen, J., Xie, W., Kuo, J., Lu, X., Chang, K., Wen, S., Sun, G., Cai, H., Buyukada, M., Evrendilek, F., 2018a. Combustion behaviors of spent mushroom substrate using TG-MS and TG-FTIR: thermal conversion, kinetic, thermodynamic and emission analyses. Bioresour. Technol. 266, 389–397.

Huang, L., Xie, C., Liu, J., Zhang, X., Chang, K., Kuo, J., Sun, J., Xie, W., Zheng, L., Sun, S., Buyukada, M., Evrendilek, F., 2018b. Influence of catalysts on co-combustion of sewage sludge and water hyacinth blends as determined by TG-MS analysis. Bioresour. Technol. 247, 217–225.

Liang, F., Wang, R., Hongzhong, X., Yang, X., Zhang, T., Hu, W., Mi, B., Liu, Z., 2018. Investigating pyrolysis characteristics of moso bamboo through TG-FTIR and Py-GC/MS. Bioresour. Technol. 256, 53–60.

Lin, Y., Liao, Y., Yu, Z., Fang, S., Lin, Y., Fan, Y., Peng, X., Ma, X., 2016. Co-pyrolysis kinetics of sewage sludge and oil shale thermal decomposition using TGA–FTIR analysis. Energy Convers. Manage. 118, 345–352.

López-González, D., Parascanu, M.M., Fernandez-Lopez, M., Puig-Gamero, M., Soreanu, G., Avalos-Ramírez, A., Valverde, J.L., Sanchez-Silva, L., 2017. Effect of different concentrations of O_2 under inert and CO_2 atmospheres on the swine manure combustion process. Fuel 195, 23–32.

Ma, Z., Zhi, W., Ye, J.W., Zhang, Q., 2015. Determination of pyrolysis characteristics and kinetics of rice husk using TGA-FTIR and model-free integral methods. Shengwu Huaxue Gongcheng 49 (3), 27–32.

Maia, Amanda Alves Domingos, Morais, L.C.D., 2016. Kinetic parameters of red pepper waste as biomass to solid biofuel. Bioresour. Technol. 204, 157–163.
Meng, F., Yu, J., Tahmasebi, A., Han, Y., 2013. Pyrolysis and combustion behavior of coal gangue in O_2/CO_2 and O_2/N_2 mixtures using thermogravimetric analysis and a drop tube furnace. Energy Fuels 27 (6), 2923–2932.
Moussout, H., Ahlafi, H., Aazza, M., Bourakhouadar, M., 2016. Kinetics and mechanism of the thermal degradation of biopolymers chitin and chitosan using thermogravimetric analysis. Polym. Degrad. Stabil. 130, 1–9.
Pelvan, E., Özilgen, M., 2017. Assessment of energy and exergy efficiencies and renewability of black tea, instant tea and ice tea production and waste valorization processes. Sustain. Product. Consump. 12, 59–77.
Selcuk, N., Yuzbasi, N.S., 2011. Combustion behaviour of Turkish lignite in O_2/N_2 and O_2/CO_2 mixtures by using TGA–FTIR. J. Anal. Appl. Pyrolysis 90, 133–139.
Shen, B., Tian, L., Li, F., Zhang, X., Xu, H., Singh, S., 2017. Elemental mercury removal by the modified bio-char from waste tea. Fuel 187, 189–196.
Tang, Y., Ma, X., Lai, Z., Zhou, D., Chen, Y., 2013. Thermogravimetric characteristics and combustion emissions of rubbers and polyvinyl chloride in N_2/O_2 and CO_2/O_2 atmospheres. Fuel 104, 508–514.
Tang, Y., Ma, X., Wang, Z., Wu, Z., Yu, Q., 2017. A study of the thermal degradation of six typical municipal waste components in CO_2 and N_2 atmospheres using TGA-FTIR. Thermochim. Acta 657, 12–19.
Tian, L., Shen, B., Xu, H., Li, F., Wang, Y., Singh, S., 2016. Thermal behavior of waste tea pyrolysis by TG-FTIR analysis. Energy 103, 533–542.
Tran, K.-Q., Bach, Q.-V., Trinh, T.T., Seisenbaeva, G., 2014. Non-isothermal pyrolysis of torrefied stump – a comparative kinetic evaluation. Appl. Energy 136, 759–766.
urmanova1, S.Ch., Genieva, S.D., Dimitrova, A.S., Vlaev, L.T., 2008. Non-isothermal degradation kinetics of filled with rise huskash polypropene composites. Express. Polym. Lett. 2, 133–146.
Uzun, B.B., Apaydin-Varol, E., Ateş, F., Özbay, N., Pütün, A.E., 2010. Synthetic fuel production from tea waste: characterisation of bio-oil and bio-char. Fuel 89, 176–184.
Wall, T., Liu, Y., Spero, C., Elliott, L., Khare, S., Rathnam, R., Zeenathal, F., Moghtaderi, B., Buhre, B., Sheng, C., Gupta, R., Yamada, T., Makino, K., Yu, J., 2009. An overview on oxyfuel coal combustion—state of the art research and technology development. Chem. Eng. Res. Des. 87, 1003–1016.
Wang, H., Chen, X., Ding, L., Qiu, F., Zhang, Q., Cai, Z., Kong, X., 2016. Contents of main components and metal ions in tea raw materials and tea waste from different kinds of instant tea. Zhongguo Nongxue Tongbao 36 (29), 53–57.
Wang, S., Wang, K., Liu, Q., Gu, Y., Luo, Z., Cen, K., Fransson, T., 2009. Comparison of the pyrolysis behavior of lignins from different tree species. Biotechnol. Adv. 27, 562–567.
Wen, L., Tao, Q., OU, Y., Gao, F., Yang, Z., Chen, J., Xu, Y., 2016. Comparison of calorific value of agro-forestry biomass and optimal formula of tobacco stem-cornstalk briquette (in Chinse). Hunan Nongye Kexue, 1, 43–46.
Xie, C., Liu, J., Xie, W., Kuo, J., Lu, X., Zhang, X., He, Y., Sun, J., Chang, K., Xie, W., Liu, C., Sun, S., Buyukada, M., Evrendilek, F., 2018a. Quantifying thermal decomposition regimes of textile dyeing sludge, pomelo peel, and their blends. Renewable Energy 122, 55–64.
Xie, W., Wen, S., Liu, J., Xie, W., Kuo, J., Lu, X., Sun, S., Chang, K., Buyukada, M., Evrendilek, F., 2018b. Comparative thermogravimetric analyses of co-combustion of textile dyeing sludge and sugarcane bagasse in carbon dioxide/oxygen and nitrogen/oxygen atmospheres: thermal conversion characteristics, kinetics, and thermodynamics. Bioresour. Technol. 255, 88–95.
Yao, F., Tao, J., Wang, H., Hu, G., Chen, S., Hussian, T.M., 2017. Study of pyrolysis behavior and reaction mechanism of tea polyphenols. Linchan Huaxue yu Gongye 37 (5), 19–27.
Yuan, X., He, T., Cao, H., Yuan, Q., 2017. Cattle manure pyrolysis process: Kinetic and thermodynamic analysis with isoconversional methods. Renewable Energy 107, 489–496.
Zhang, Z., Wang, C., Huang, G., Liu, H., Yang, S., Zhang, A., 2018. Thermal degradation behaviors and reaction mechanism of carbon fibre-epoxy composite from hydrogen tank by TG-FTIR. J. Hazard. Mater. 357, 73–80.
Zhao, T., Chen, Z., Lin, X., Ren, Z., Li, B., Zhang, Y., 2018. Preparation and characterization of microcrystalline cellulose (MCC) from tea waste. Carbohydr. Polym. 184, 164–170.
Zhao, J., Xiuwen, W., Hu, J., Liu, Q., Shen, D., Xiao, R., 2014. Thermal degradation of softwood lignin and hardwood lignin by TG-FTIR and Py-GC/MS. Polym. Degrad. Stabil. 108, 133–138.
Zhuo, Z., Liu, J., Sun, S., Sun, J., Kuo, J., Chang, K., Fu, J., Wang, Y., 2017. Thermogravimetric characteristics of textile dyeing sludge, coal and their blend in N_2/O_2 and CO_2/O_2 atmospheres. Appl. Therm. Eng. 111, 87–94.
Zhong, L., Tang, X., Shao, Z., Wang, X.X., 2017. Production and application of tea residue biomass granule fuel. Yinliao Gongye 20 (1), 50–53.